Hindawi
Advances in Civil Engineering
Volume 2019, Article ID 8156432, 13 pages
https://doi.org/10.1155/2019/8156432

Research Article

Comparative Study on Mechanical Properties of a Tube-Crushing Dissipator and a Symmetric Tube-Crushing Dissipator

Wenkang Wang[1], **Shaoqing Shi**[1], **and Gaosheng Wang**[2]

[1]*Department of Civil Engineering, Army Logistics University of PLA, Chongqing 401311, China*
[2]*63926 Army of PLA, Beijing 100000, China*

Correspondence should be addressed to Shaoqing Shi; ssq601@163.com

Received 11 August 2018; Revised 4 November 2018; Accepted 12 March 2019; Published 3 April 2019

Academic Editor: Giovanni Garcea

The tube-crushing dissipator is widely used in engineering, but it has the eccentricity problem. Therefore, a symmetric tube-crushing dissipator was proposed in this article, and quasistatic and dynamic tests were performed to compare mechanical properties of the tube-crushing dissipators and the symmetric tube-crushing dissipators. The results of the quasistatic tests show that the working force of the tube-crushing dissipators fluctuates around an average value which is about 20% smaller than the activation threshold after activation, while the working force fluctuates around an average value which is approximately equal to the activation threshold after activation. The results of the dynamic tests show that mean force at the crushing section of the tube-crushing dissipators and the symmetric tube-crushing dissipators increases with the increase of the impact velocity. Furthermore, the dynamic load-displacement curves are more volatile than those of the static tests. Therefore, dynamic tests which are more similar to the real working conditions of the dissipators are preferable over static tests. In addition, the metal tubes of the symmetric tube-crushing dissipators collapse vertically both in the quasistatic and dynamic tests; that is, the eccentricity problem of the tube-crushing dissipators is overcome by the symmetric tube-crushing dissipators.

1. Introduction

Rockfall hazards occur frequently in mountainous areas, which are potential dangers to transportation facilities and human safety. A great amount of rockfall retention systems with different retention capacities are adopted to mitigate or eliminate the consequences of rockfall hazards, such as rigid walls [1], active and passive flexible net systems [2], flexible rock-sheds [3], etc. Among the above technological solutions, passive flexible net systems are the most widely used solutions due to their wide retention capacity range, which are composed of steel posts, steel nets, supporting and anchoring ropes, and energy dissipators.

The energy dissipators are the devices that limit the maximum forces acting on the anchorage and absorb parts of the impact energy of the rockfalls by pure friction, partial failure, plastic deformation, or mixed friction and plastic deformation [4]. Ring brake, double-U ring brake, U-shape dissipator, and the tube-crushing dissipator are the most widely used dissipators in rockfall engineering (Figure 1), wherein, the mechanical properties of the ring brake [5], double-U ring brake [6], and U-shape dissipator [7] have been investigated, while there is little research regarding the tube-crushing dissipator.

To better understand the energy-absorption mechanism and capacity of the energy dissipators, both quasistatic and dynamic tests are needed. The quasistatic tests are mainly performed in a horizontal or vertical traction machine, with one cable end of the dissipator fixed and the other cable end pulled [7–10]. The aim of the dynamic tests is to approximate more to real conditions, and the tests can be conducted in the following three ways. The first way is to fix one cable end of the energy dissipator to a hanging point and connect the other cable end to a block, and then the block is hoisted to a certain height and dropped freely [10, 11]. The second way is to connect the energy dissipator to a horizontal cable anchored at both ends and let a block vertically impact the cable [12, 13]. The last way is to study the dynamic behavior

(a) (b) (c) (d)

Figure 1: The most widely used dissipators in rockfall engineering. (a) Ring brake. (b) Double-U ring brake [6]. (c) U-shape dissipator. (d) Metal-tube-crushing dissipator.

of energy dissipators by carrying out an in situ impact test on a full barrier [14]. Among the above three ways, the first way is more operable for its simplicity.

The metal-tube-crushing dissipator is composed of two metal tubes, two steel cables, and two rigid perforated plugs at the ends, as shown in Figure 2(a). The steel cables pass through the tubes with one end fixed by aluminum sleeves outside the perforated plugs. When impacted by rockfalls, the two steel cables move in opposite directions, which makes the plugs press against the metal tubes. The metal tubes buckle under the pressure of perforated plugs with plastic deformation and absorb energy at the same time. A circular tube may deform in an axisymmetric mode, nonsymmetric mode, mixed mode, or Euler mode, which mainly depends on its diameter, thickness, and length [16]. The axisymmetric mode theory was first proposed by Alexander [17] and developed by Abramowicz and Jones [18, 19], Grzebieta [20], etc. The nonsymmetric mode was studied by Pugsley and Macaulay [21], Abramowicz and Jones [18, 19], Singace [22], etc. All these theories could provide reference for the design of the metal-tube-crushing dissipators.

Former research shows that the tube-crushing dissipator has the problem of torque generation because of eccentricity [15], which may cause the collapse mode of metal tube changes from vertical collapse to oblique collapse and increase the difficulty of energy dissipation analysis, as shown in Figure 2(b). Therefore, the main purpose of this article is to propose a symmetric tube-crushing dissipator to overcome the existing problems of the tube-crushing dissipator and compare static and dynamic mechanical properties of the tube-crushing dissipator and the symmetric tube-crushing dissipator by static and dynamic tests, which will provide reference for the design and engineering application of the symmetric tube-crushing dissipators.

2. Proposal of a Symmetric Tube-Crushing Dissipator

To overcome the eccentricity problem of the tube-crushing dissipator, a symmetric tube-crushing dissipator was proposed in this article, which had been applied for a patent [23]. The symmetric tube-crushing dissipator is composed of four steel cables, four circular metal tubes, and two plugs at the end, as shown in Figure 3. The plugs are cuboid metal blocks with two sets of symmetric counterbore holes, which are used to constrain the ends of metal tubes and pass through the steel cables. The steel cables pass through the metal tubes, with one end anchored outside the plug by aluminum sleeves and the other end passing through the plug at the other side symmetrically. Steel cables passing through the same plug are combined together by the aluminum sleeves, and the resultant force lies on the central connecting line of the plugs.

3. Quasistatic and Dynamic Tests

3.1. Quasistatic Tests. The quasistatic tests of the tube-crushing dissipators and the symmetric tube-crushing dissipators were performed on a RGM-100KN universal test machine and a WAW-1000KN universal test machine, respectively, as shown is Figure 4. The 304 stainless steel tubes were used in the quasistatic tests, and parameters of the tubes are listed in Table 1. Considering the size of the energy dissipators, the tensile distance in the static tests was set to 200 mm. The static tests were controlled by the displacement rate with a value of 20 mm/min. The tests were divided into three groups according to the thickness of the metal tubes, and three test samples of the same batch were selected for the same group of tests.

3.2. Dynamic Tests. The dimensions of the tube-crushing dissipators and the symmetric tube-crushing dissipators used in the dynamic tests were consistent with those in the static test, and the thickness of the metal tubes was 0.4 mm. The experimental setup of the dynamic tests is shown in Figure 5. The force sensor is hung on the steel beam which was fixed to the reaction frames. One steel cable end of the energy dissipator is connected to the sensor hung on the steel beam, and the other end is connected to the rockfall. The rockfall is a precast sphere block with a diameter of 0.4 m and a mass of 80 kg. The rockfall was hoisted by a crane to a certain height and released by an automatic pneumatic release device. The vertical height from the steel beam to the ground is about 5.0 m. Considering the lengths of the dissipators and limitations of the connecting steel cables, three dynamic tests of the tube-crushing dissipators and two dynamic tests of the symmetric tube-crushing dissipators were conducted, respectively, and the free-falling distances were controlled by the lift heights and the cable lengths. If the vertical height is too small, the dissipator cannot be activated. If the vertical height is too big, the dissipator will

(a) (b)

Figure 2: Pictures of the tube-crushing dissipator [15]: (a) before use; (b) after use.

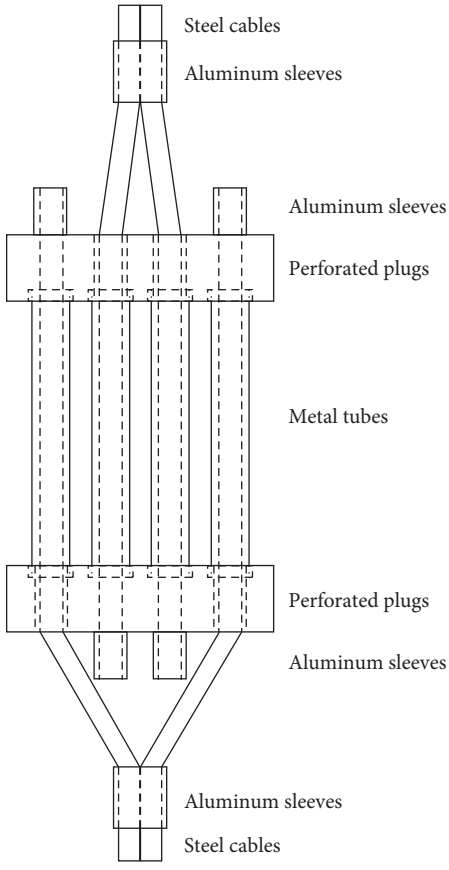

Figure 3: Scheme of the symmetric tube-crushing dissipator.

hit the ground before activation. The free-falling distances and initial impact velocities of the rockfall in the dynamic tests were calculated using the time span from the rockfall release to the steel cables in tension recorded by the high-speed camera, as listed in Table 2. To make the data more accurate, future work of more tests and numerical simulations validated by tests should be conducted.

The dynamic data acquisition system includes a force sensor, a strain adaptor, a dynamic data acquisition instrument, and a high-speed camera (see Figure 6). The force sensor used in the test has a range of 0–200 kN and a sensitivity of 1.4484 mV/V. The TEST3810 strain adaptor was used to transfer the voltage data. The TEST6200 dynamic data acquisition instrument with a sampling frequency of 20 kHz was used to record the dynamic data, which was processed by an accompanying software in the laptop. A Sony camera with a speed of 300 frames/s was used to record the entire impact process.

4. Results and Discussion

4.1. Static Test Results

4.1.1. Result Analysis. Although the thicknesses of the metal tubes are different, the static tensile processes of the three groups for each type are almost the same, as shown in Figures 7 and 8. The load-displacement curves obtained from the static tests are shown in Figures 9 and 10, and the average load-displacement curves are shown in Figure 11.

Taking the tensile load-displacement curve of sample 1(tube-crushing dissipator) with a metal tube thickness of 0.5 mm as an example, the quasistatic tensile process of the tube-crushing dissipator and the symmetric tube-crushing dissipator can be divided into three sections, as shown in Figure 12. The first section is the activation section or the elastic section, where the force increases linearly with the increase of the displacement until the load reaches the activation force threshold of the energy dissipator. After the force reaches the activation force threshold, the load-displacement curve rapidly drops and forms a trough. Under the action of the pulling force, the energy dissipator continuously buckles to form folds, and the load-displacement curve forms new wave peaks and troughs. The section could be called the crushing section, which is also the main energy absorption section of the dissipators. The last section is the failure section, where the metal tubes fully collapse, and the load-displacement curve rises sharply. The system behaves like a single cable because it is the steel cables that bear the load.

The energy absorbed by the energy dissipators can be calculated according to integral of the load-displacement curves obtained from the tests [14], which is expressed as follows:

(a) (b)

Figure 4: Experimental setup of the quasistatic tests. (a) Tube-crushing dissipator. (b) Symmetric tube-crushing dissipator.

Table 1: Parameters of the 304 stainless steel tubes.

Density (kg/m^3)	Yield stress (MPa)	Length (mm)	Outer diameter (mm)	Thickness (mm)
7850	402	200	22	0.4, 0.5, 0.55

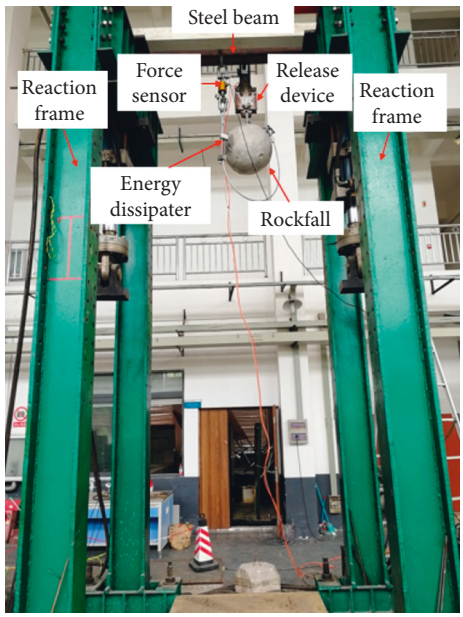

Figure 5: Experimental setup of the dynamic tests.

$$W = \int_0^s F(\delta) \cdot d\delta, \tag{1}$$

where δ denotes the tensile displacement of the energy dissipator, $F(\delta)$ denotes the load corresponding to the displacement δ, and s denotes the maximum displacement of the crushing section.

Table 2: Free-falling distances and initial impact velocities in the dynamic tests.

Type	Tube-crushing dissipator			Symmetric tube-crushing dissipator	
Free-falling distance (m)	2.78	3.35	3.58	2.94	3.73
Initial impact velocity (m/s)	7.38	8.10	8.38	7.59	8.46

Therefore, the average force at crushing section of the energy dissipators can be obtained by the following formula:

$$F_m = \frac{\int_{L_1}^{L_2} F(\delta) \cdot d\delta}{L_2 - L_1}, \tag{2}$$

where F_m denotes the average force at crushing section, δ denotes the tensile displacement of the energy dissipator, and L_1 and L_2 denote the start displacement and finish displacement of the crushing section, respectively.

The activation force threshold, absorbed energy, and mean force at the crushing section of the dissipators are the main mechanical parameters related to engineering application, and the values of which for the tube-crushing dissipators and the symmetric tube-crushing dissipators in the

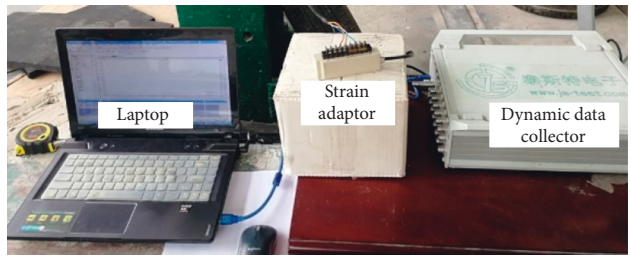

Figure 6: Dynamic data acquisition system.

(a) (b) (c)

Figure 7: The quasistatic tensile process of the tube-crushing dissipator.

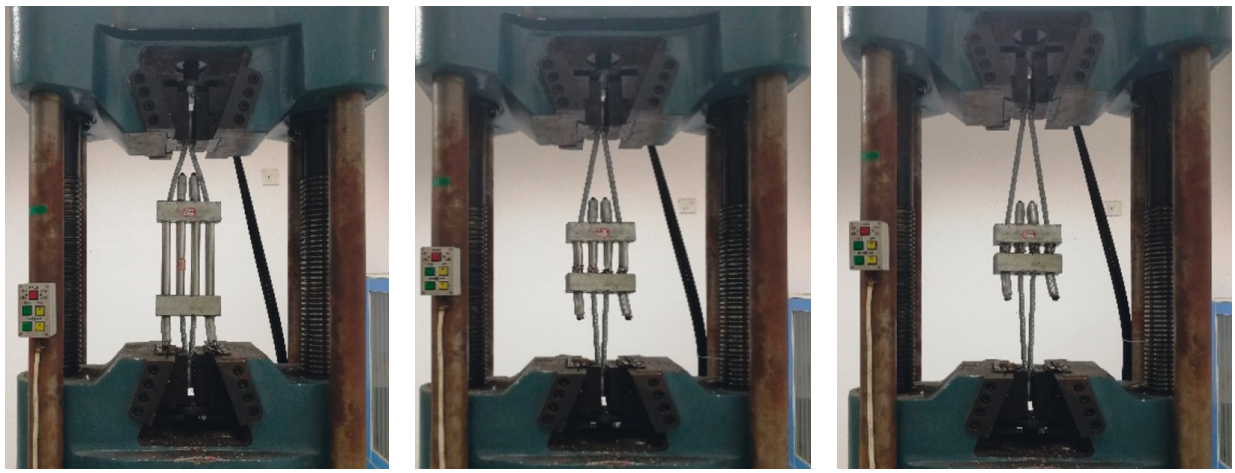

(a) (b) (c)

Figure 8: The quasistatic tensile process of the symmetric tube-crushing dissipator.

static tests are listed in Tables 3 and 4. As can be seen from Table 3, the mean activation force thresholds of the tube-crushing dissipators of different tube thicknesses are 10.82 kN, 15.45 kN, and 17.77 kN, respectively, and the mean forces at the crushing section of different tube thicknesses are 8.56 kN, 12.13 kN, and 13.69 kN, respectively. The latter are about 79.1%, 78.5%, and 77.0% of the former. As can be seen from Table 4, the mean activation force thresholds of the symmetric tube-crushing dissipators of different tube thicknesses are 23.07 kN, 29.02 kN, and 33.34 kN, respectively, and the mean forces at the crushing section of different tube thicknesses are 20.57 kN, 29.46 kN, and 31.12 kN, respectively.

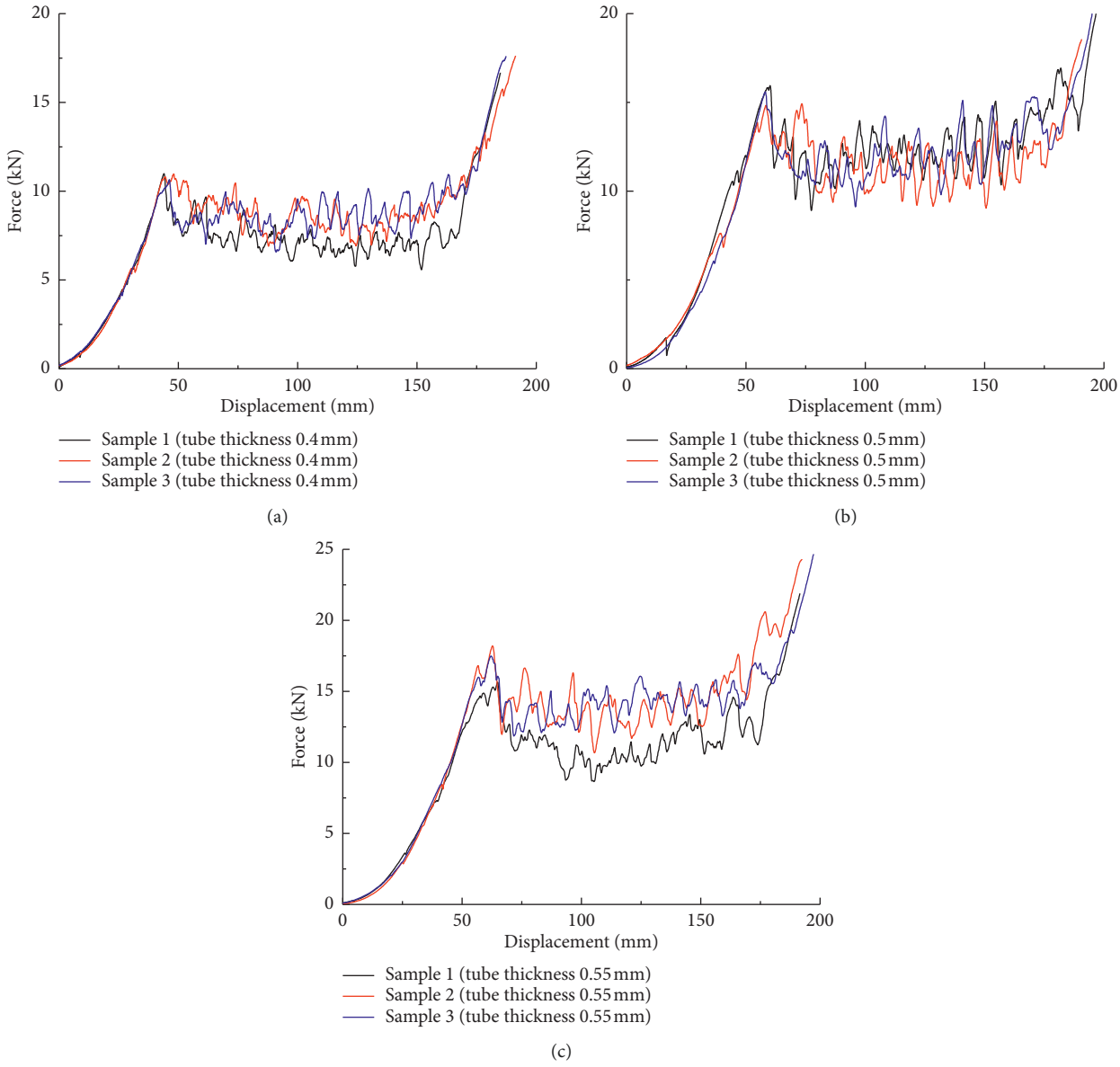

Figure 9: Quasistatic tensile load-displacement curves of the tube-crushing dissipators with different tube thicknesses: (a) 0.4 mm, (b) 0.5 mm, and (c) 0.55 mm.

The latter are about 89.2%, 101.5%, and 93.3% of the former. Apparently, the activation force thresholds and the mean forces at the crushing section of the tube-crushing dissipators and the symmetric tube-crushing dissipators increase with the thickness of the metal tubes. For the tube-crushing dissipators, the working force decreases obviously after activation and then fluctuates around an average value which is about 20% smaller than the activation threshold. For the symmetric tube-crushing dissipators, the working force fluctuates around an average value which is approximately equal to the activation threshold after activation.

4.2. Dynamic Test Results. Figure 13 shows the typical impact process of the tube-crushing dissipators and the symmetric tube-crushing dissipators. After released by the pneumatic release system, the rockfall fell freely until the steel cables of the dissipator were in tension. The upper plug moved downward due to the traction of the steel cables, while the lower plug remained stationary. As a result, the metal tubes were crushed and the energy was dissipated.

The dynamic tensile load-time curves of the tube-crushing dissipators and the symmetric tube-crushing dissipators obtained from the tests are shown in Figures 14 and 15, and the pictures of the dissipators after dynamic impact are shown in Figures 16 and 17. Similar to the static tensile load-displacement curves, the dynamic tensile load-time curves can also be divided into the activation section, the crushing section, and the failure section. If the tubes collapse fully before the rockfall stops, the failure section could be found in the dynamic load-time curve, where the curve rises sharply to a peak and goes down until the rockfall stops, as

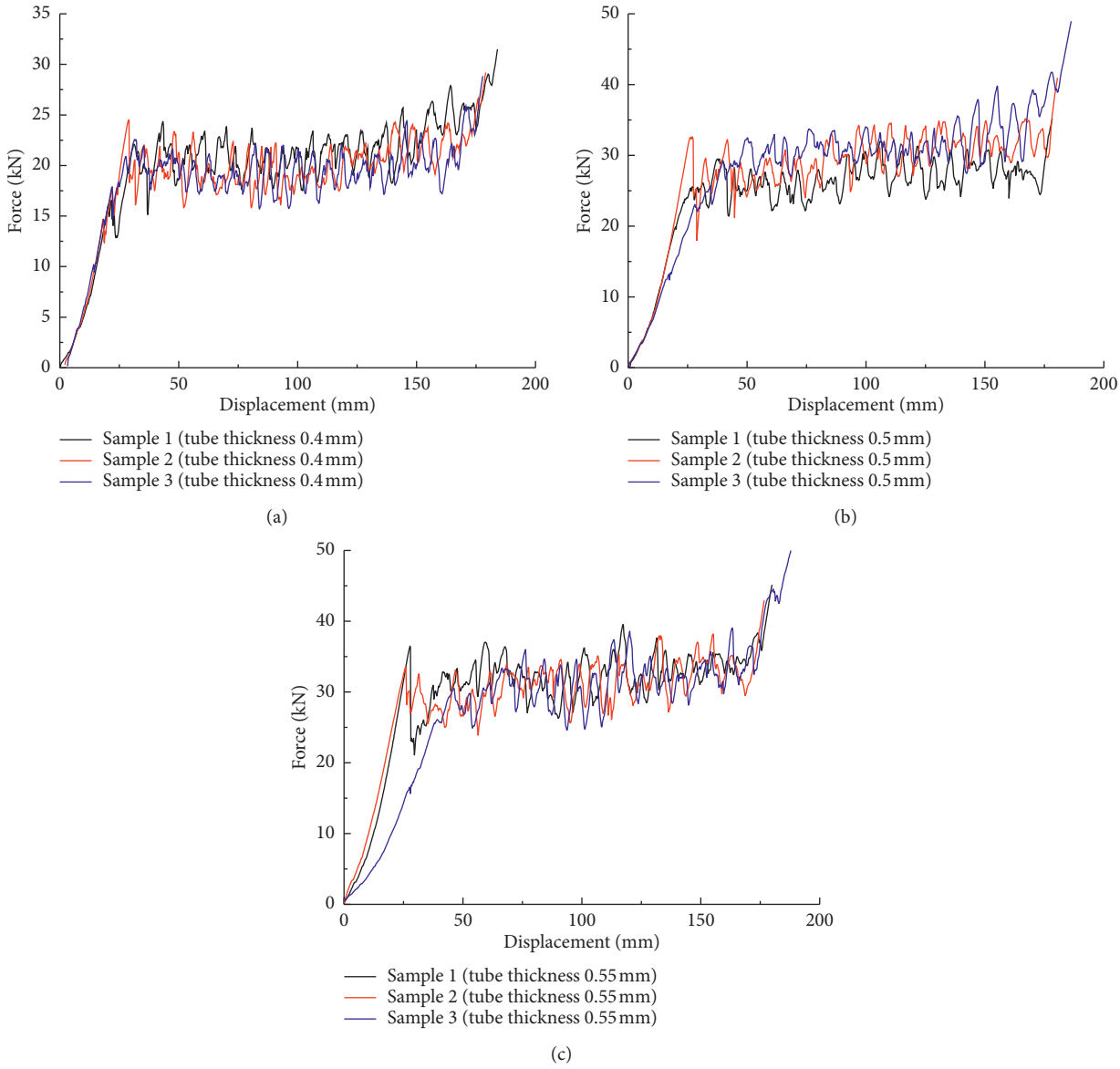

Figure 10: Quasistatic tensile load-displacement curves of the symmetric tube-crushing dissipators with different tube thicknesses: (a) 0.4 mm, (b) 0.5 mm, and (c) 0.55 mm.

shown in Figures 14(a) and 16(a). Otherwise, there would not be the failure section in the dynamic load-time curve, and the curve forms wave peaks and troughs smoothly until the rockfall stops, as shown in Figures 14(b) and 16(b). The dynamic compression times were the time span from the dissipator activation to the tubes full collapse or the rockfall stop. When the full-scale barriers were hit by rockfalls, dissipators mounted on steel cables will also experience a similar process in the dynamic tests of this article.

The compression distances of the dissipators were recorded after the dynamic tests, and the total energy absorbed during the dynamic test could be calculated using the free-falling distances of the rockfall and the compression distances of the dissipators, as listed in Tables 5 and 6.

The motion direction and the perforated plug positions of the dissipators changed all the time during the impact process. Though the dynamic tests were recorded using a high-speed video camera, the time-distance curves extracted from the videos are not so accurate. In the dynamic tests, the force fluctuates around an average value after activation approximately. Therefore, a constant deceleration results in a linear velocity decrease of the block and parabolic braking curve over time. To simplify the data processing, the supposition of a linear relationship between displacement and time is adopted in this article [11], and the accuracy should be validated by numerical simulations. Therefore, the load-time curves of the tube-crushing dissipators and the symmetric tube-crushing dissipators obtained from dynamic tests could be converted to the load-displacement curves, as shown in Figures 18 and 19.

Similarly, the activation force threshold, absorbed energy, and mean force at the crushing section of the dissipators could be obtained using formulas (1) and (2), and the results are listed in Tables 5 and 6. As can be seen from

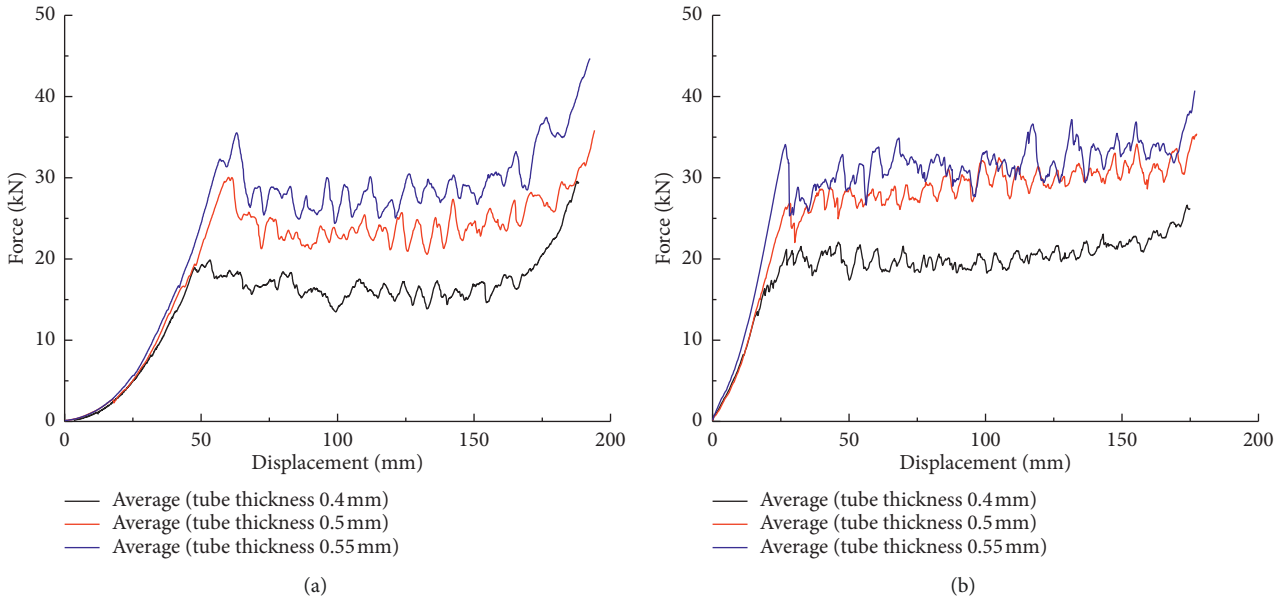

Figure 11: Average quasistatic tensile load-displacement curves of the dissipators with different tube thicknesses. (a) Tube-crushing dissipators. (b) Symmetric tube-crushing dissipators.

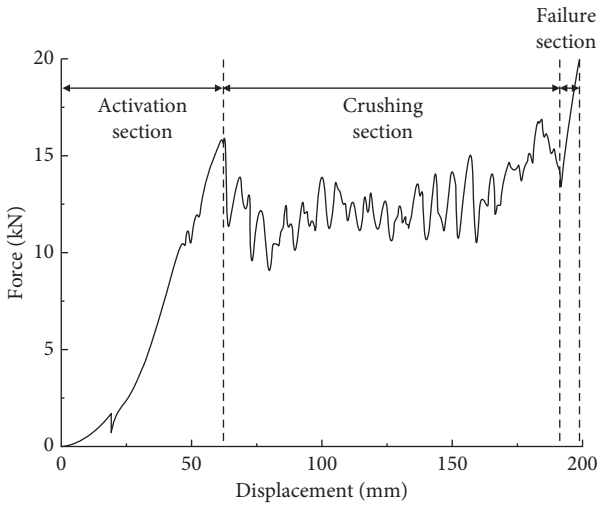

Figure 12: Typical load-displacement curve of the tube-crushing dissipator and the symmetric tube-crushing dissipator in the quasistatic test.

Table 5, the active force thresholds of the tube-crushing dissipators with an initial velocity of 7.38 m/s, 8.10 m/s, and 8.38 m/s are 15.20 kN, 16.95 kN, and 18.36 kN, respectively, and mean forces at the crushing section are 11.11 kN, 17.36 kN, and 17.94 kN, respectively. The latter are about 73.1%, 102.4%, and 97.7% of the former. As can be seen from Table 6, the active force thresholds of the symmetric tube-crushing dissipators with an initial velocity of 7.59 m/s and 8.55 m/s are 22.05 kN and 24.07 kN, respectively, and the mean forces at the crushing section are 21.85 kN and 24.06 kN, respectively. The latter are about 99.1% and 99.9% of the former. Furthermore, mean force at the crushing section of the tube-crushing dissipators and the symmetric tube-crushing dissipators increases with the increase of the impact velocity. Mean force at the crushing section with an initial velocity of 7.38 m/s, 8.10 m/s, and 8.38 m/s increases by 29.7%, 102.7%, and 109.4%, respectively, contrast to that of the static tests for the tube-crushing dissipators, and the mean force at the crushing section with an initial velocity of 7.59 m/s and 8.55 m/s increases by 9.6% and 17.0%, respectively. In addition, the dynamic load-displacement curves are more volatile than those of the static tests. Therefore, dynamic tests which are more similar to the real working conditions of the dissipators should be performed before engineering application.

5. Discussion

In quasistatic tests, mean forces at the crushing section of the dissipators increase with the thickness of the metal tubes. In dynamic tests, mean force at the crushing section of the dissipators increases with the increase of the impact velocity, while the tube thickness remains the same. Combing with these two conclusions, mean forces at the crushing section of the dissipators increase with tube thickness when velocity remains the same; mean forces at the crushing section of the metal-tube-crushing dissipators increase with impact velocity when tube thickness remains the same.

As can be seen from Figures 7 and 16, the two steel cables of the tube-crushing dissipator are not in a straight line. Torque generates under the action of the pulling force because of eccentricity; as a result, the perforated plugs deflect during the tensile process. Therefore, the vertical relationship between perforated plugs and metal tubes shifts, and the metal tube collapse mode changes from vertical collapse to oblique collapse, which increases the difficulty of energy dissipation and energy consumption analysis of the dissipator. In addition, local stress occurs at the contact between the steel cables and the plugs. The sliding friction

Table 3: Main mechanical parameters of the tube-crushing dissipators at static tests.

Tube thickness (mm)	No.	Activation force threshold (kN)	Absorbed energy (kJ)	Mean force at the crushing section (kN)
0.4	Sample 1	10.99	1.18	8.24
	Sample 2	10.81	1.24	8.73
	Sample 3	10.66	1.28	8.72
	Average	10.82	1.23	8.56
0.5	Sample 1	15.94	2.00	12.64
	Sample 2	14.83	1.74	11.62
	Sample 3	15.59	1.75	12.13
	Average	15.45	1.83	12.13
0.55	Sample 1	17.60	1.85	12.69
	Sample 2	18.21	1.90	14.04
	Sample 3	17.49	2.09	14.33
	Average	17.77	1.95	13.69

Table 4: Main mechanical parameters of the symmetric tube-crushing dissipators at static tests.

Tube thickness (mm)	No.	Activation force threshold (kN)	Absorbed energy (kJ)	Mean force at the crushing section (kN)
0.4	Sample 1	22.15	3.42	21.62
	Sample 2	24.46	3.14	20.08
	Sample 3	22.61	3.05	20.01
	Average	23.07	3.20	20.57
0.5	Sample 1	25.55	4.26	26.84
	Sample 2	32.45	4.82	29.81
	Sample 3	29.05	5.09	31.75
	Average	29.02	4.72	29.46
0.55	Sample 1	36.32	5.17	30.21
	Sample 2	33.35	4.85	31.11
	Sample 3	30.35	5.02	32.03
	Average	33.34	5.01	31.12

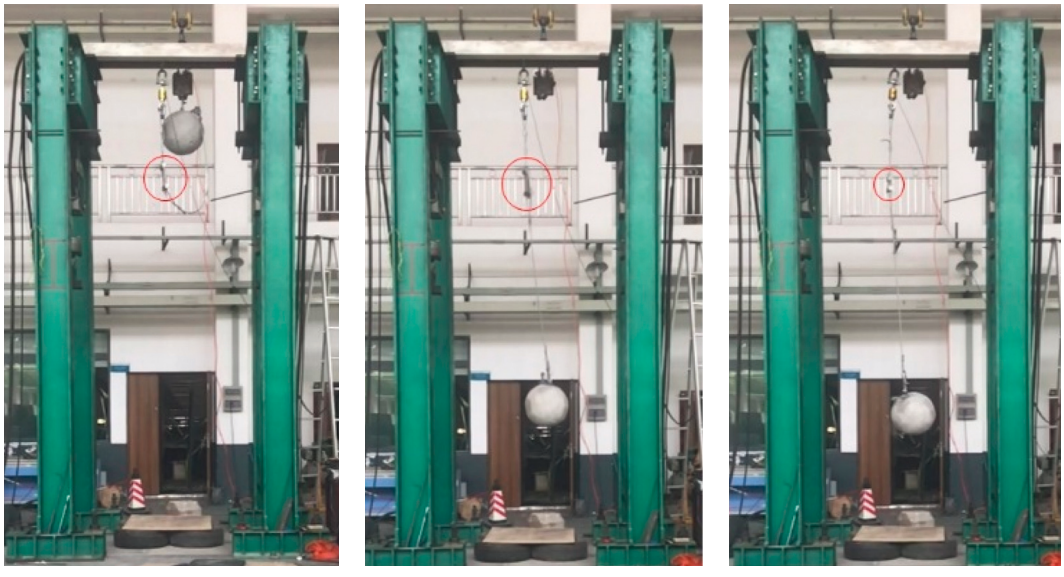

(a) (b) (c)

Figure 13: Dynamic impact process of a symmetric tube-crushing dissipator.

between the steel cables and plugs may cause local abrasion or even breakage of the steel cables, which is a potential safety danger, as shown in Figure 20.

As can be seen from Figures 8 and 17, the steel cables of the symmetric tube-crushing dissipators are symmetric, and the resultant force of the dissipators lies on the central

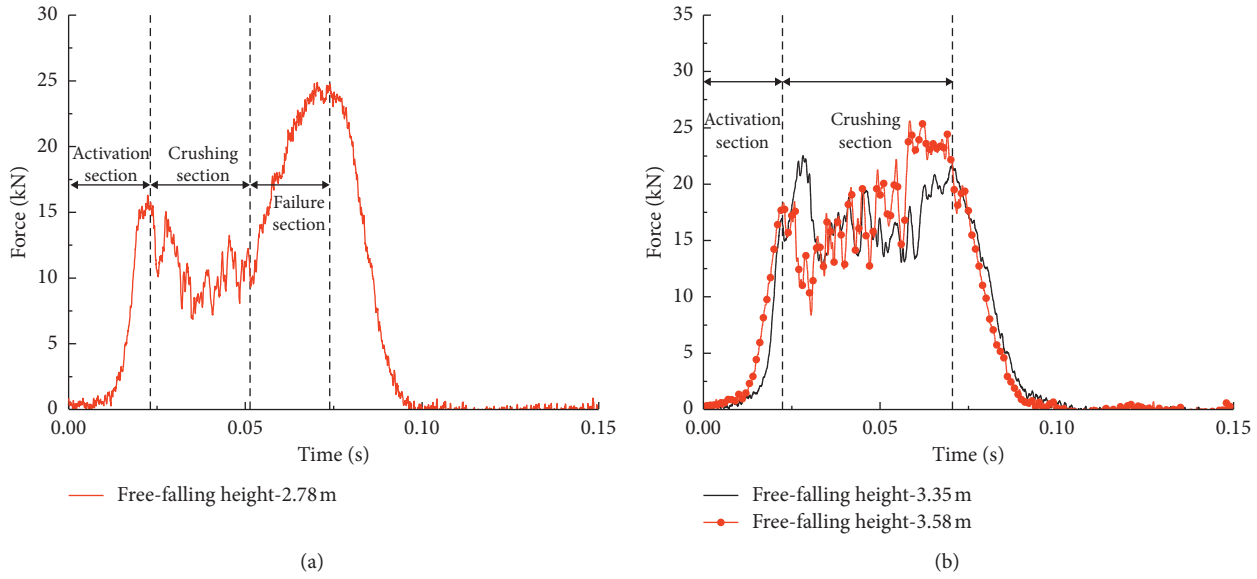

Figure 14: Dynamic load-time curves of the tube-crushing dissipators.

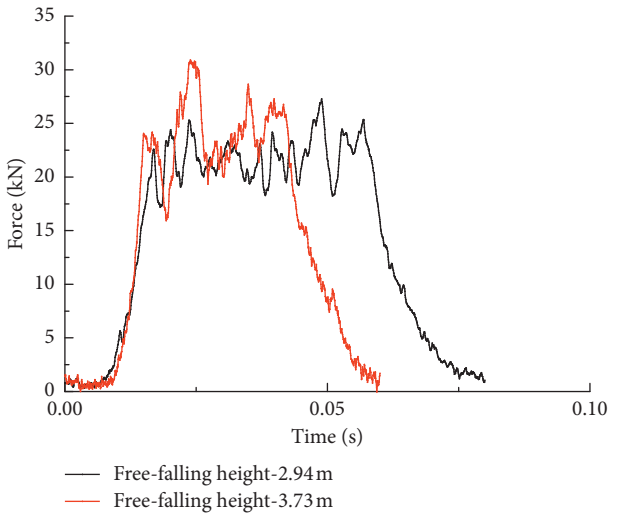

Figure 15: Dynamic load-time curves of the symmetric tube-crushing dissipators.

connecting line of the plugs. The metal tubes collapse vertically both in the quasistatic and dynamic tests, and the friction between the steel cables and the plugs could be negligible. That is, the eccentricity problem of the tube-crushing dissipators is overcome by the symmetric tube-crushing dissipators.

6. Conclusions

To overcome the eccentricity problem of the tube-crushing dissipator, a symmetric tube-crushing dissipator was proposed. Then, static and dynamic tests were performed to compare mechanical properties of the tube-crushing dissipators and the symmetric tube-crushing dissipators, and the following conclusions could be drawn:

(1) The quasistatic tensile process of the dissipators can be divided into three sections, that is, the activation section, the crushing section, and the failure section. Herein, the crushing section is the main energy absorption section of the dissipators. Furthermore, the mean forces at the crushing section are about 79.1%, 78.5%, and 77.0% of the activation force thresholds for the tube-crushing dissipators, which means the working force decreases obviously after activation and then fluctuates around an average value which is about 20% smaller than the activation threshold. The mean forces at the crushing section are about 89.2%, 101.5%, and 93.3% of the activation force thresholds for the symmetric tube-crushing dissipators, which means the working force fluctuates around an average value which is approximately equal to the activation threshold.

(2) The dynamic tensile load-time curves of the dissipators can also be divided into the activation section, the crushing section, and the failure section. Furthermore, mean force at the crushing section of the tube-crushing dissipators and the symmetric tube-crushing dissipators increases with the increase of the impact velocity. Mean force at the crushing section with an initial velocity of 7.38 m/s, 8.10 m/s, and 8.38 m/s increases by 29.7%, 102.7%, and 109.4%, respectively, contrast to that of the static tests for the tube-crushing dissipators, and mean force at the crushing section with an initial velocity of 7.59 m/s and 8.55 m/s increases by 9.6% and 17.0%, respectively. In addition, the dynamic load-displacement curves are more volatile than those of the static tests. Therefore, dynamic tests which are more similar to

(a) (b)

Figure 16: Tube-crushing dissipators after dynamic impact. (a) Tubes fully collapsed. (b) Tubes not fully collapsed.

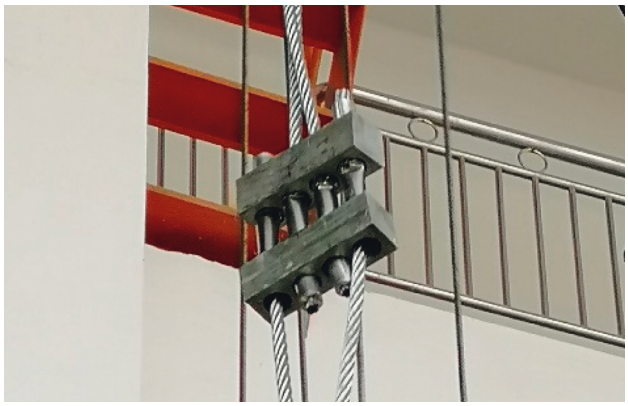

Figure 17: Symmetric tube-crushing dissipators after dynamic impact.

Table 5: Parameters of the tube-crushing dissipators in the dynamic tests.

No.	Free-falling distance (m)	Impact velocity (m/s)	Compression distance of the dissipator (m)	Total energy (kJ)	Activation force (kN)	Absorbed energy (kJ)	Mean force at the crushing section (kN)	Braking time (s)
Test 1	2.78	7.38	0.18	2.32	15.20	1.76	11.11	0.05
Test 2	3.35	8.10	0.16	2.75	16.95	2.34	17.36	0.07
Test 3	3.58	8.38	0.16	2.93	18.36	2.48	17.94	0.07

Table 6: Parameters of the symmetric tube-crushing dissipators in the dynamic tests.

No.	Free-falling distance (m)	Impact velocity (m/s)	Compression distance of the dissipator (m)	Total energy (kJ)	Activation force (kN)	Absorbed energy (kJ)	Mean force at the crushing section (kN)	Braking time (s)
Test 1	2.94	7.59	0.12	2.45	22.05	2.32	21.85	0.06
Test 2	3.73	8.55	0.13	3.11	24.07	2.85	24.06	0.09

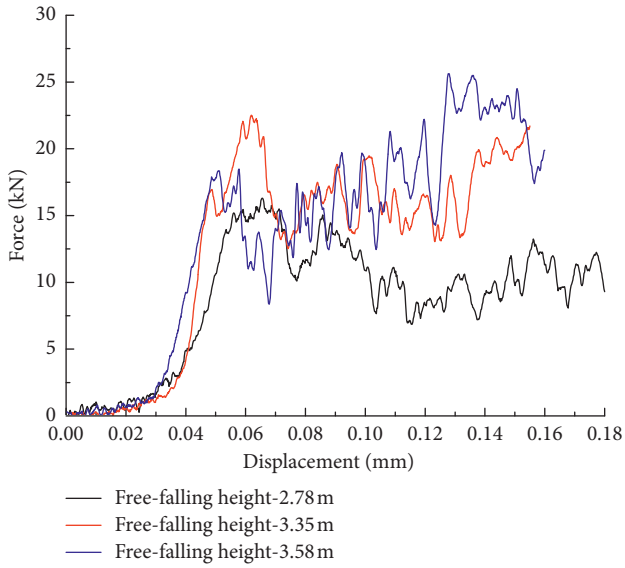

Figure 18: Dynamic tensile load-displacement curves of the tube-crushing dissipators.

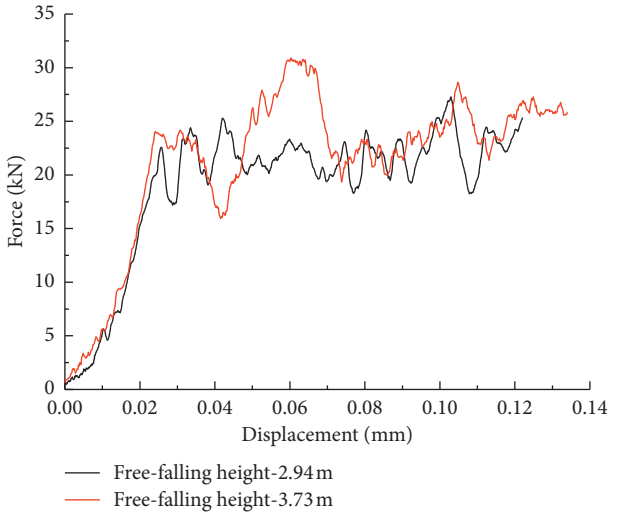

Figure 19: Dynamic tensile load-displacement curves of the symmetric tube-crushing dissipators.

the real working conditions of the dissipators are preferable over static tests.

(3) Torque generates under the action of the pulling force because of eccentricity for the tube-crushing dissipators, and the perforated plugs deflect during the tensile process. Also, local stress occurs at the contact between the steel cables and the plugs. The sliding friction between the steel cables and plugs may cause local abrasion or even breakage of the steel cables, which is a potential safety danger. For the symmetric tube-crushing dissipators, the metal tubes collapse vertically both in the quasistatic and dynamic tests, and the friction between the steel cables and the plugs could be negligible. That is, the eccentricity problem of the tube-crushing dissipators is overcome by the symmetric tube-crushing dissipators.

Figure 20: Abrasion of steel cables for tube-crushing dissipators after tests.

Data Availability

The data used to support the findings of this study are available from the corresponding author upon request.

Conflicts of Interest

The authors declare that there are no conflicts of interest regarding the publication of this paper.

References

[1] A. Volkwein, K. Schellenberg, V. Labiouse et al., "Rockfall characterisation and structural protection-a review," *Natural Hazards and Earth System Sciences*, vol. 11, no. 9, pp. 2617–2651, 2011.

[2] S. Q. Shi, M. Wang, X. Q. Peng, and Y. K. Yang, "A new-type flexible rock-shed under the impact of rock block: initial experimental insights," *Natural Hazards and Earth System Sciences*, vol. 13, no. 12, pp. 3329–3338, 2013.

[3] W. K. Wang, S. Q. Shi, Y. F. Liu, and G. S. Wang, "The application of expanded polystyrene cushion layer in oblique flexible net systems for rockfall protection: a new attempt," *International Journal of Protective Structures*, vol. 9, no. 2, pp. 141–156, 2018.

[4] L. Castanon-Jano, E. Blanco-Fernandez, D. Castro-Fresno, and F. Ballester-Muñoz, "Energy dissipating devices in falling rock protection barriers," *Rock Mechanics and Rock Engineering*, vol. 50, no. 3, pp. 603–619, 2017.

[5] M. Wang, S. Q. Shi, and Y. K. Yang, "Static tensile test and FEM dynamic simulation for a ring-brake energy disspater," *Journal of Vibration and Shock*, vol. 30, no. 4, pp. 188–193, 2011, in Chinese.

[6] J. J. del Coz Díaz, P. J. García Nieto, D. Castro-Fresno, and J. Rodríguez-Hernández, "Nonlinear explicit analysis and study of the behaviour of a new ring-type brake energy dissipator by FEM and experimental comparison," *Applied Mathematics and Computation*, vol. 216, no. 5, pp. 1571–1582, 2010.

[7] M. Wang, S. Q. Shi, L. M. Cui et al., "Mechanical performance analysis on U-brake energy dissipator used in passive protection nets," *Engineering Mechanics*, vol. 33, no. 6, pp. 114–119, 2016, in Chinese.
[8] D. Peila, S. Pelizza, and F. Sassudelli, "Evaluation of behaviour of rockfall restraining nets by full scale tests," *Rock Mechanics and Rock Engineering*, vol. 31, no. 1, pp. 1–24, 1998.
[9] D. Castro-Fresno, J. J. del Coz Díaz, P. J. García Nieto et al., "Comparative analysis of mechanical tensile tests and the explicit simulation of a brake energy dissipator by FEM," *International Journal of Nonlinear Sciences and Numerical Simulation*, vol. 10, no. 8, pp. 1059–1085, 2009.
[10] D. Bertrand, A. Trad, A. Limam et al., "Full-scale dynamic analysis of an innovative rockfall fence under impact using the discrete element method: from the local scale to the structure scale," *Rock Mechanics and Rock Engineering*, vol. 45, no. 5, pp. 885–900, 2012.
[11] A. Trad, L. Ali, B. David et al., "Multi-scale Analysis of an innovative flexible rockfall barrier," in *Rockfall Engineering*, pp. 303–342, Wiley, New York, NY, USA, 2011.
[12] K. Kawakami, K. Shinohara, M. Iwasaki et al., "Evaluation of pocket-type rock net by full scale tests," *IABSE Symposium Report*, vol. 96, no. 4, pp. 10–19, 2009.
[13] P. V. Tran, K. Maegawa, and S. Fukada, "Experiments and dynamic finite element analysis of a wire-rope rockfall protective fence," *Rock Mechanics and Rock Engineering*, vol. 46, no. 5, pp. 1183–1198, 2013.
[14] M. Fulde and M. Müller, "Development of a modular brake element for the use in modern rockfall catchment fences," in *Proceedings of 64th Highway Geology Symposium Highway Geology Symposium*, North Conway, NH, USA, September 2013.
[15] C. Gentilini, G. Gottardi, L. Govoni, A. Mentani, and F. Ubertini, "Design of falling rock protection barriers using numerical models," *Engineering Structures*, vol. 50, pp. 96–106, 2013.
[16] X. Huang and G. Lu, "Axisymmetric progressive crushing of circular tubes," *International journal of crashworthiness*, vol. 8, no. 1, pp. 87–95, 2003.
[17] J. M. Alexander, "An approximate analysis of the collapse of thin cylindrical shells under axial loading," *Quarterly Journal of Mechanics and Applied Mathematics*, vol. 13, no. 1, pp. 10–15, 1960.
[18] W. Abramowicz and N. Jones, "Dynamic axial crushing of circular tubes," *International Journal of Impact Engineering*, vol. 2, no. 3, pp. 263–281, 1984.
[19] W. Abramowicz and N. Jones, "Dynamic progressive buckling of circular and square tubes," *International Journal of Impact Engineering*, vol. 4, no. 4, pp. 243–270, 1986.
[20] R. H. Grzebieta, "An alternative method for determining the behaviour of round stocky tubes subjected to an axial crush load," *Thin-Walled Structures*, vol. 9, no. 1–4, pp. 61–89, 1990.
[21] A. Pugsley and M. Macaulay, "The large-scale crumpling of thin cylindrical columns," *Quarterly Journal of Mechanics and Applied Mathematics*, vol. 13, no. 1, pp. 1–9, 1960.
[22] A. A. Singace, "Axial crushing analysis of tubes deforming in the multi-lobe mode," *International Journal of Mechanical Sciences*, vol. 41, no. 7, pp. 865–890, 1999.
[23] Z. W. Shi, S. Q. Shi, and W. K. Wang, "An energy dissipation device made of metal tubes,"' CN107988927A, 2018, in Chinese.